

Structure, defects, and strain in silicon-silicon oxide interfaces

Goran Kovačević^{a)} and Branko Pivac

Department of Materials Physics, Rudjer Boskovic Institute, Bijenička 56, P.O.B. 180,
HR-10002 Zagreb, Croatia

(Received 16 October 2013; accepted 8 January 2014; published online 31 January 2014)

The structure of the interfaces between silicon and silicon-oxide is responsible for proper functioning of MOSFET devices while defects in the interface can deteriorate this function and lead to their failure. In this paper we modeled this interface and characterized its defects and strain. MD simulations were used for reconstructing interfaces into a thermodynamically stable configuration. In all modeled interfaces, defects were found in the form of three-coordinated silicon atom, five coordinated silicon atom, threefold-coordinated oxygen atom, or displaced oxygen atom. Three-coordinated oxygen atom can be created if dangling bonds on silicon are close enough. The structure and stability of three-coordinated silicon atoms (P_b defect) depend on the charge as well as on the electric field across the interface. The negatively charged P_b defect is the most stable one, but the electric field resulting from the interface reduces that stability. Interfaces with large differences in periodic constants of silicon and silicon oxide can be stabilized by buckling of silicon layer. The mechanical stress resulted from the interface between silicon and silicon oxide is greater in the silicon oxide layer. *Ab initio* modeling of clusters representing silicon and silicon oxide shows about three time larger susceptibility to strain in silicon oxide than in silicon if exposed to the same deformation. © 2014 AIP Publishing LLC. [<http://dx.doi.org/10.1063/1.4862809>]

I. INTRODUCTION

Silicon is an intrinsic semiconductor which can be technologically produced in the most pure form as a single element. Its electronic properties can be fine-tuned in the wide range by intentional doping with specific elements.¹ Moreover, surface-oxidation produces a silicon dioxide (SiO_2); a stable and uniform material with large band gap, which can serve as a high quality insulator. Modern techniques succeed in producing precise, atomically flat surfaces of silicon,^{1,2} covered with SiO_2 layer, only several atomic layers thick.³

These properties make silicon a unique element, suitable for building metal-oxide semiconductor field-effect transistor (MOSFET),⁴ a *building-block* device for explosive development of information and communication technologies in the several last decades. Therefore it makes the interface between silicon and SiO_2 (Si-SiO_2) technologically one of the most important atomic interfaces.⁵ Properties of MOSFET devices are greatly influenced by the Si-SiO_2 interface since charged defects that might be present there could significantly alter its properties; therefore, understanding the structure and defects at Si-SiO_2 interfaces is important for further development of electronic devices, especially with constant shrinking of the SiO_2 thickness.^{4,6} While silicon, used in manufacture of electronic devices, is crystalline, thermally grown SiO_2 is amorphous,^{6,7} and the interface is abrupt and smooth.⁸ Nevertheless, there are indications about the ordered crystalline structure of the SiO_2 close to the Si-SiO_2 interface.^{8–11}

At the interface region, there should be at least one layer of silicon atoms that are bonded both with oxygen and silicon atoms. These silicon atoms are in the intermediate

oxidation states (+1, +2, +3, depending on the number of oxygen atoms they are bound to).^{12,13} The presence of these silicon atoms with intermediate states is referred as a chemical stress¹⁴ while mismatch in periodic constants is a source of the mechanical stress.^{8,11,15,16} The interface layer is also found to be a source of structural defects that are electrically active and are responsible for degradation of performances of MOS devices upon exposure to high electrical currents or ionizing radiation. The most important one is the P_b defect.^{17–19} It is identified as a silicon atom with a dangling bond $[\text{Si}(3)]$.^{15,20–22} The presence of this defect is easily identified with the EPR spectroscopy.²³ $\text{Si}(3)$ is amphoteric, i.e., it can be present in positive $[\text{Si}(3)^+]$, neutral $[\text{Si}(3)^0]$, and negative state $[\text{Si}(3)^-]$.²⁴ Their populations depend on their energy, relative to the Fermi level. Since only $\text{Si}(3)^0$ is paramagnetic, only this species is detected in EPR spectra. $\text{Si}(3)^0$ has an energy in the mid-gap, between valence and conductive bands of silicon. Increasing or lowering the Fermi level extinguishes the EPR signal since $\text{Si}(3)^0$ is being depopulated. According to Lenahan and Conley,²³ $\text{Si}(3)^+$ has lower and $\text{Si}(3)^-$ has higher energy relative to $\text{Si}(3)^0$.

Despite tremendous importance and intensive studies of the interface between these two materials, there are still many unknowns in the structure of that interface. In our previous paper,²⁵ we took five models for the interfaces between the silicon [100] surface and different forms of silicon oxide and challenged them by simulating an exposure to high temperatures and slowly cooling them down. Chosen temperatures were high enough to alter the bonding pattern in strained bonds at interfaces, but too low for melting either silicon or silicon oxide matrix. The procedure of heating and slowly cooling was used in order to drive system toward the energetically more stable state.

^{a)}Electronic mail: gkova@irb.hr. Tel./Fax: +385 01 4561486.

In this paper our aim is to characterize interfaces with other silicon surfaces ([110] and [111]) and investigate strain and defects that are the result of interfacing. Consequently, we created models for interfaces with Si[110] and Si[111] for β -cristobalite (β c), and β -quartz (β q) as well as interfaces with amorphous silicon oxide forms (Figure 1).

This paper is organized as follows: In Sec. II, computational methods for preparation of modeled interfaces are described. In Sec. III, atomistic structure of interfaces is reported. In Sec. IV observed defects are described and analyzed, and finally in Sec. V stress in interfaces is calculated.

II. COMPUTATIONAL METHODS

We used the Reax force field (ReaxFF)²⁶ to model and characterize interfaces between Si [110] and [111] surfaces and different phases of crystalline and amorphous SiO_2 . While traditional force fields have restrictions on a very narrow part of potential energy surfaces, close to energy minima, the ReaxFF was designed to accurately describe

geometries that are far from the equilibrium including processes such as bond breaking, molecular isomerization, change of atom coordination or change in molecular conformation. In this work, we used parameters, developed by van Duin *et al.*^{27,28} for silicon and silicon oxide systems (ReaxFF_{SiO}). This force field was parametrized against accurate quantum chemical and periodic DFT calculations and can describe cases where oxygen and/or silicon is under- or over-coordinated or systems with silicon involved in double or triple bonds. The ability of the ReaxFF_{SiO} force field to predict the stability of SiO_2 polymorphs was also demonstrated by van Duin *et al.*²⁷

A. Preparation of models: Crystalline interfaces

In order to study the interface between crystalline Si and crystalline SiO_2 we created modeled systems in which a slab of crystalline silicon was sandwiched between two crystalline silicon-oxide slabs. Crystal lattices of silicon and silicon-oxide were prepared by replicating their primitive cells. Crystal

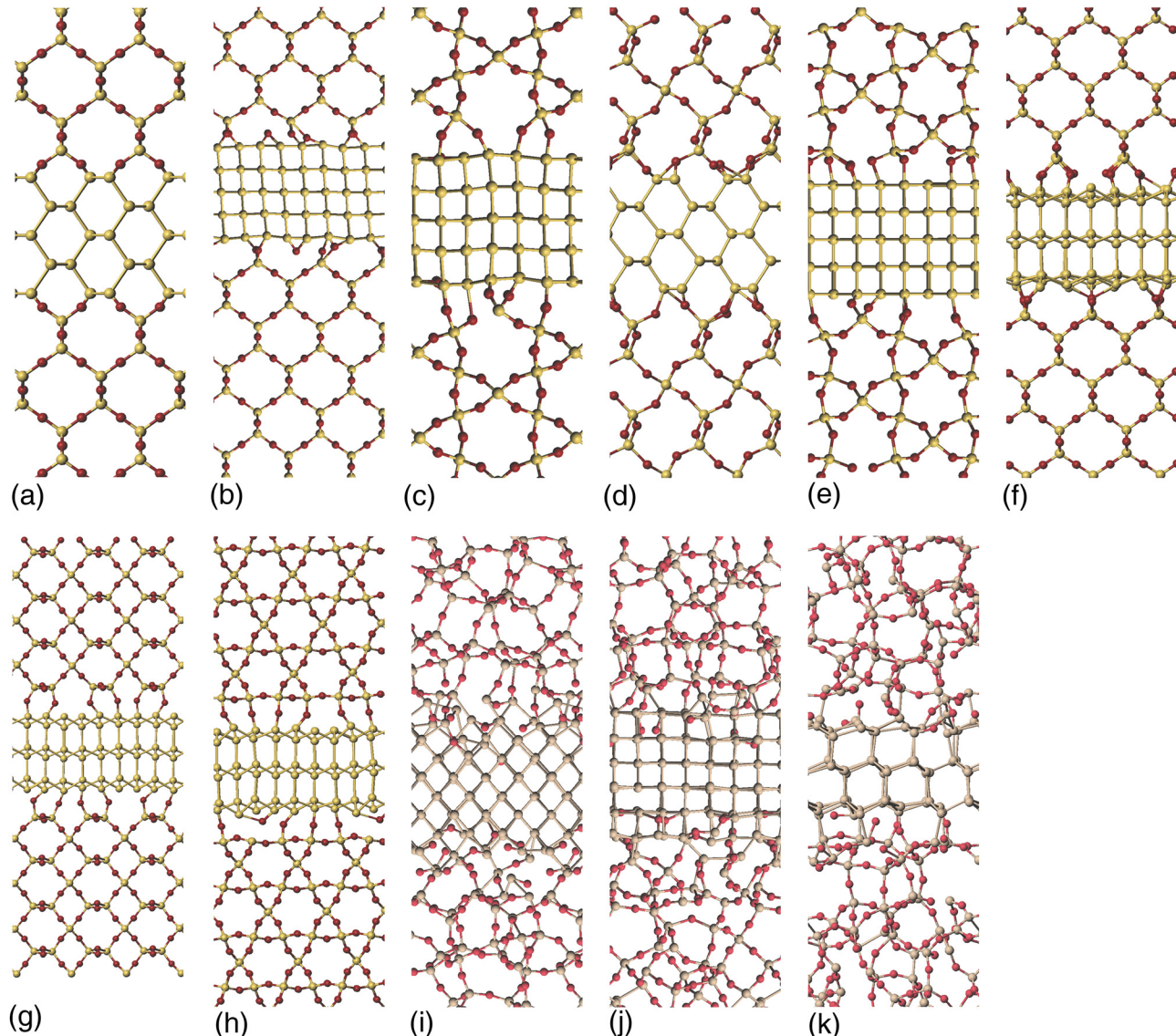


FIG. 1. Model systems of the ideal interfaces between silicon and silicon oxide layers. (a) c SiO_2 [110]A; (b) c SiO_2 [110]B; (c) q SiO_2 [110]A; (d) q SiO_2 [110]B; (e) q SiO_2 [110]C; (f) c SiO_2 [111]; (g) q SiO_2 [111]A; (h) q SiO_2 [111]B; (i) a SiO_2 [100]; (j) a SiO_2 [110]; (k) a SiO_2 [111].

lattices of silicon were rotated before cutting them into slabs in order to make [110] and [111] surfaces along the upper and the lower boundary. All silicon and silicon-oxide samples were cut in orthogonal shape. Pairs of silicon and silicon-oxide lattices were chosen according to their unit cell sizes. Only pairs whose unit cell dimensions were similar in x and y directions were chosen since their orthogonal super-cells could be stacked. Since we want models without boundaries, introduced by cutting of crystal lattices, we employed periodic boundary conditions in all three dimensions. In order to be able to impose periodic boundary conditions without breaking chemical bonds, x and y dimensions of silicon and silicon-oxide pairs must match exactly. Therefore we compressed the larger cell in silicon and silicon-oxide pair and elongated the shorter one. The silicon slab cannot be arbitrarily stacked with silicon-oxide one. By translating the silicon slab in x and y directions relative to the corresponding layers of silicon-oxide, it is possible to find the relative position of these super-cells where the number of chemical bonds between atoms in the silicon super-cell and atoms in the silicon-oxide super-cell is maximal. Since we implied periodic boundary conditions to our models, translated silicon slab was always perfectly stacked between silicon-oxide super-cells. After the number of bonds in interfaces was maximized, positions of atoms in interfaces were shifted by editing their coordinates in order to reduce the strain in elongated bonds. If interfaces contained valence-unsatisfied silicon atoms, oxygen atoms were introduced between them, if possible.

Such prepared systems were subjected to a series of geometry optimizations and low-temperature molecular dynamics (MD) simulations. Geometry optimization relaxes the system by reducing forces acting on atoms, and low temperature MD simulations were used to relax the system by changing unit cell parameters. After relaxation, the temperature of the silicon oxide layers was increased to 1000 K over 15 ps. The temperature of 1000 K is too low for melting the silicon or any of silicon oxide forms considered, but is high enough for atom rearrangements to take place in the Si–SiO₂ interface region. The MD simulation was performed on the system for 50 ps after which the system was cooled for another 50 ps at the cooling rate of 1.94×10^{13} K s⁻¹. Geometry optimization was performed on the final geometry. Periodic boundary conditions were applied in all three dimensions, in all calculations. The time integration step of 0.5 fs was used with the velocity-Verlet integrator in all MD steps. The temperature

and the pressure were maintained with the Nose–Hoover thermostat/barostat. Temperature thermostating constant of 500 fs and pressure barostating constant 1500 fs were used. The pressure of 1 atm was kept in all MD steps. Charges, used in the reax force field for energy calculation were extracted to characterize atom bonding in the silicon–silicon oxide interfaces. Charges in reax force field were calculated by electron equilibration method, and parameters used are $\gamma(\text{Si}) = 0.8925 \text{ Å}$, $\gamma(\text{Si}) = 4.6988 \text{ eV}$, $\eta(\text{Si}) = 6.0000 \text{ eV}$, $\gamma(\text{O}) = 1.0898 \text{ Å}$, $\gamma(\text{O}) = 8.5000 \text{ eV}$, and $\eta(\text{O}) = 8.3122 \text{ eV}$. All MD calculations were done with the LAMMPS program package. The unit cell dimensions, silicon layer thickness, and total number of atoms in unit cells are shown in Table I, and the constructed model of interfaces are shown in Figure 1.

B. Preparation of models: Amorphous interface

The interfaces with stacking silicon Si[100], Si[110], and Si[111] layers sandwiched between amorphous SiO₂ (aSiO₂) were also constructed. The methodology for obtaining aSiO₂–Si–aSiO₂ systems is different from the methodology used in construction interfaces between silicon and crystalline SiO₂ (cSiO₂).^{29,30} aSiO₂ has no periodicity and size of model can be chosen arbitrarily. We used silicon super-cells that we have prepared for stacking with cSiO₂ and prepared samples of aSiO₂ that match dimensions of these silicon super-cells. The samples of amorphous SiO₂ were constructed by simulation of heating the sample of β tridymite. β tridymite was chosen since its density is close to the density of aSiO: 2.30. The periodic constants of the unit cell were adjusted in order to exactly match the density of aSiO₂ (2.20 g cm^{-3}). The system was heated from 0 K to 3500 K over 5 ps. After that, the temperature of 3500 K was maintained for next 5 ps. In that period, atoms moved from their initial positions and mixed. The system was finally cooled from 3500 K to 10 K and optimized. During MD steps atoms in silicon slab were kept frozen. All calculations with amorphous SiO₂ were conducted with constant temperature and volume conditions, and the same thermostating constant was used as in the case of interfaces with cSiO₂.

III. RESULTS AND DISCUSSION

A. Atomic structure of interfaces

Different models for the interfaces between silicon surfaces and different forms of silicon oxide are created in

TABLE I. Parameters of model systems used in simulations of Si–cSiO₂ interfaces. All unit cells are orthorhombic. N is the number of atoms in a unit cell; s is the thickness of silicon layer; Δx and Δy are mismatches in x and y directions.

Silicon oxide (model)	Silicon surface	Unit cell size/Å	N	s/Å	Δx (SiO ₂) (%)	Δy (SiO ₂) (%)	Δx (Si) (%)	Δy (Si) (%)
β cristoballite (cSiO ₂ [110]A)	[110]	$30.40 \times 30.40 \times 34.28$	2124	7.9	2.3	3.8	-2.7	-7.3
β cristoballite (cSiO ₂ [110]B)	[110]	$30.40 \times 30.40 \times 49.09$	3024	8.2	2.2	2.5	-9.1	-2.7
β quartz (qSiO ₂ [110]A)	[110]	$22.17 \times 18.46 \times 29.80$	864	7.9	0.05	7.2	4.1	-22.2
β cristoballite (cSiO ₂ [111])	[111]	$30.40 \times 20.27 \times 36.48$	1416	6.9	-0.2	-1.1	0.6	2.4
β quartz (qSiO ₂ [111]A)	[111]	$34.12 \times 20.36 \times 41.32$	2136	6.9	-9.3	-11.1	0.8	-27.9
β quartz (qSiO ₂ [111]B)	[111]	$30.31 \times 23.19 \times 40.81$	2136	6.9	2.0	4.4	-11.6	-12.3
β quartz (qSiO ₂ [110]B)	[110]	$36.81 \times 42.63 \times 28.34$	3200	7.5	7.4	7.7	-13.4	-5.5
β quartz (qSiO ₂ [110]C)	[110]	$44.34 \times 36.99 \times 29.55$	3392	8.1	0.0	7.9	4.6	-17.8

order to characterize bonding in these interfaces and to check their stability. Unlike the models with Si[100] surface,²⁵ all silicon atoms at the Si[110] and Si[111] surfaces have only one unsatisfied valency, and in the case of Si[111] surface these atoms are separated by a relatively large distance, so oxygen atoms cannot bridge them. Since oxygen atoms, which are inserted between silicon atoms in the first layer at the Si[100] surface lower the number of free valencies at Si[100] surface, the number of valencies available for bonding with SiO₂ in Si[100] surface is lower than in Si[110] and Si[111] surfaces. That results in dangling bonds in Si[110] and Si[111] interfaces. In some models (cSiO₂[110]B, qSiO₂[110]B), dangling bonds were removed by inserting bridging oxygen atoms (Figures 1(b) and 1(c)); however, inserting a bridging oxygen atom requires rearrangements in bonding, which results in the strain in the systems. Also, inserting bridging oxygen atoms makes strained three-(Si-Si-O) and four-(Si-Si-Si-O) member rings. Therefore we considered both the systems with (Figures 1(b) and 1(c)) and

without (Figures 1(a) and 1(e)) these bridging oxygen atoms. Unfortunately, there are models in which all atoms cannot be valence-satisfied.

As in our previous paper, we used β -quartz instead of its more stable α form since β -quartz is more stable at elevated temperatures,³³ which are used in simulations of thermal treatment. Simulations of thermal treatment of modeled systems were performed in order to change bonding in the interface region, and the sequence of heating and cooling procedures was used to drive systems to the thermodynamically more stable state. In all systems, heat treatment did not disrupt the structures of the silicon and the silicon oxide layers. The only difference between initial and annealed models is in dislocated oxygen atoms and in the bonding layout in the interface region. In Figure 2 shown are interfaces with cSiO₂ after annealing. Annealed interfaces with aSiO₂ are shown in Figures 1(i)–1(k).

Unlike the case of interface between cristobalite and Si[100] surface,²⁵ no interface considered in this work has

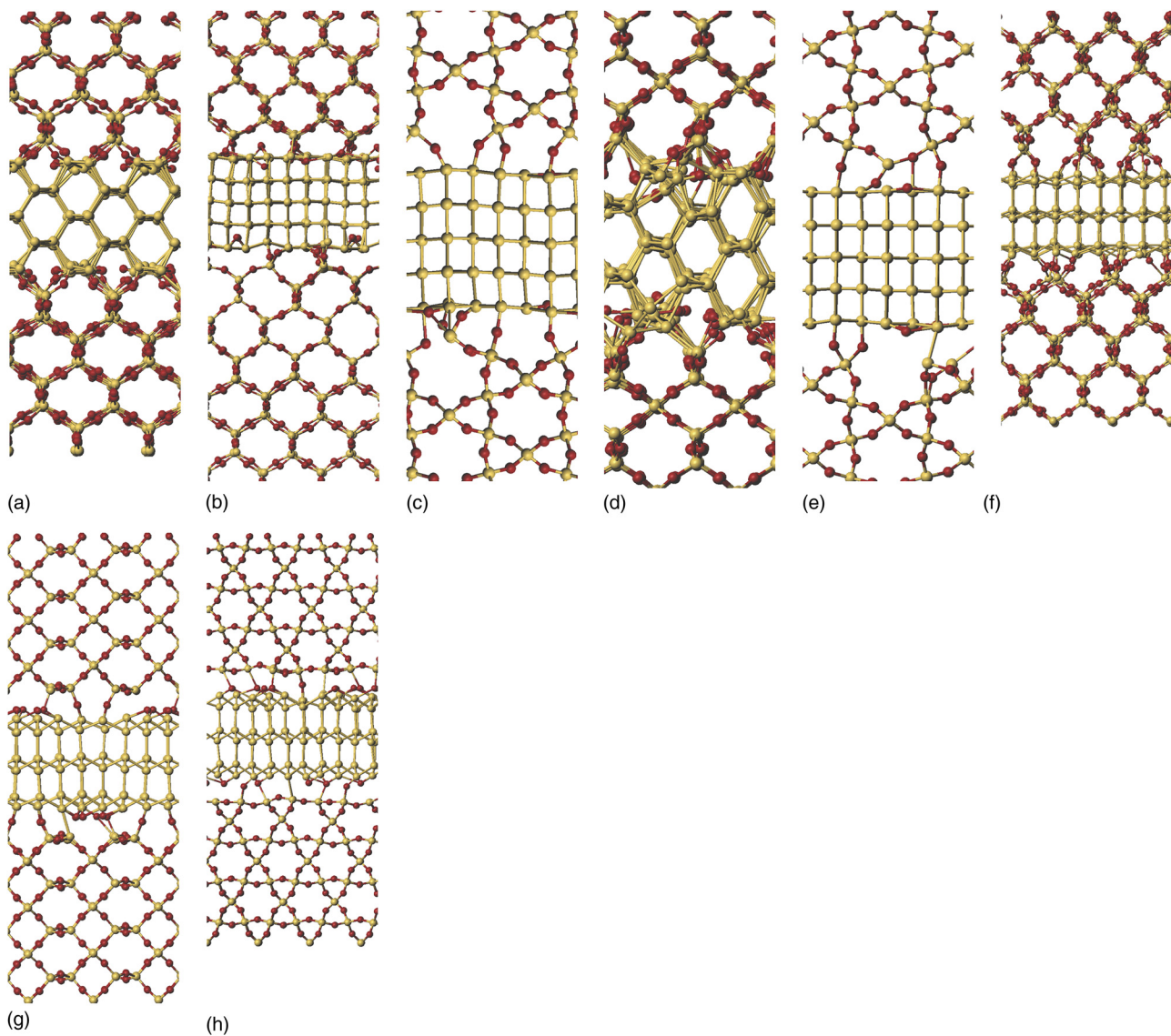


FIG. 2. The structures of the modeled interfaces after simulation of thermal treatment. (a) cSiO₂[110]A; (b) cSiO₂[110]B; (c) qSiO₂[110]A; (d) qSiO₂[110]B; (e) qSiO₂[110]C; (f) cSiO₂[111]; (g) qSiO₂[111]A; (h) qSiO₂[111]B.

been reorganized into the amorphous two-dimensional layer. However, two of the considered models have a significant mismatch in periodic constants between the two layers. In one case ($\text{qSiO}_2[110]\text{A}$) a mismatch creates buckling of the silicon layer that shapes the layer into a wavelike pattern (Figure 3(a)). That buckling is caused by introduction of oxygen atoms at the surface of the silicon layer and supported by the arrangement of atoms in the quartz layer. That arrangement pulls the silicon layer along the z coordinate in one direction and on the other spot push the silicon layer into another direction. The another case is $\text{qSiO}_2[111]\text{B}$, where a high strain between layers is supported by oxygen atoms that migrated from the surface of β -quartz to the surface of the silicon layer, where dangling bonds were present. In that case, oxygen atoms are migrating from the SiO_2 layer, towards the dangling bonds, leaving Si-Si bonds behind. These oxygen atoms are inserted between silicon centers with unsatisfied valencies making one bond, which is the regular silicon-oxygen bond (about 1.8 Å), and two bonds,

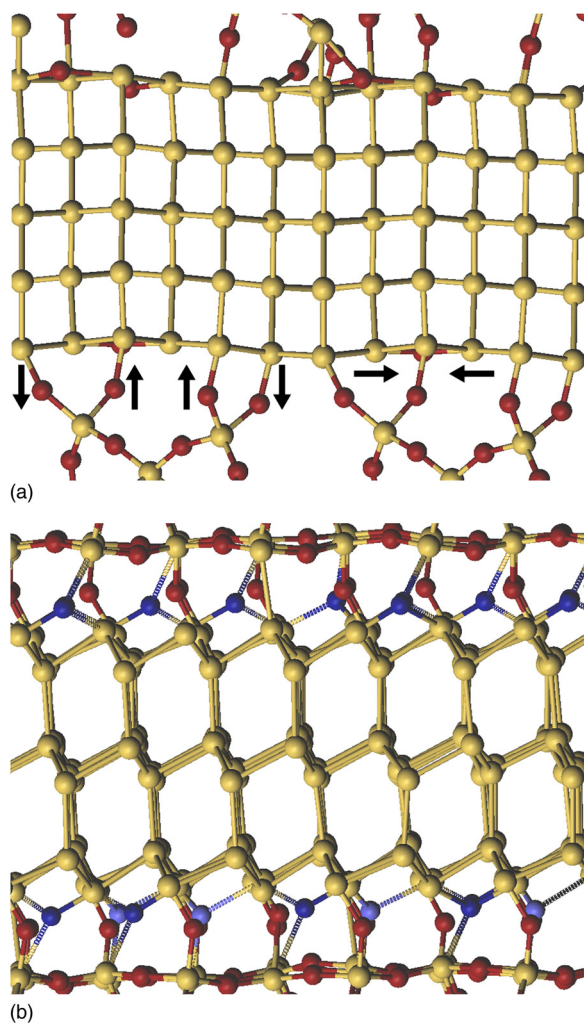


FIG. 3. (a) Buckling of the silicon layer. Buckling is caused by compression from the oxygen atoms at the surface of silicon layer (horizontal arrows) and from pulling and pushing from the quartz layer (vertical arrows). (b) Compression stabilization of the silicon layer, caused by displaced oxygen atoms. Displaced oxygen atoms are shown in blue color and partial bonds are shown as stippled cylinders. The atoms that are only partially involved in bridging the atoms in the silicon layer are depicted in light blue.

which are strained (over 2.0 Å), partial bonds (Figure 3(b)). Although silicon centers with dangling bonds are too far away for bridging by oxygen atoms, in strained systems that bridging is possible although the bonds involved in bridging are elongated.

B. The order in interfaces

The fundamental property of interfaces between Si and SiO_2 layers is appearance of silicon atoms in intermediate oxidation states. In ideal crystals of Si and SiO_2 that are free of defects, such silicon atoms do not appear. Therefore, we are using these atoms to define region of space defined by an interface and therefore a shape of an interface. In our last article we used atom charges²⁵ as a convenient method for determination of the position of silicon atoms with different oxidation states. We are not interested in absolute value of charges, but rather in the fact that silicon atoms that are connected to more oxygen atoms (more positive oxidation number) have a more positive charge since oxygen atoms drain charge by the electronegativity effect. That difference in atomic charges makes the basis for differentiation of atoms that belong to an interface from other atoms. The charges of silicon atoms, taken from ReaxFF_{SiO} calculations with particular oxidation number, are given in Table II. The exact charges may vary from these values since deformations in the coordination sphere can also make an influence. This effect is pronounced in the $\text{cSiO}_2[110]\text{A}$ and the $\text{qSiO}_2[110]\text{B}$ interfaces (Figures 4(a) and 4(c)) where the stress causes spreading of charges in the SiO_2 layer. Furthermore, as all interfaces are oriented perpendicular to z axis, in interfaces with crystalline order all atoms with the same oxidation state should be at the same z coordinate. If the interface is amorphous, this order in positions of atoms would disappear. Therefore, by plotting the dependence of atomic charges on the atomic position (along z axis), the amount of crystalline order in interface can be shown by clustering of atoms with the same charge at the same position on z coordinate. In our last paper, we showed that in the interface region of cristobalite and $\text{Si}[100]$ there is no grouping of silicon atoms with the same oxidation number to the same z coordinate, indicating that the crystalline order is disrupted.²⁵ This amorphous order is confined only to the interface regions. Here, we repeated the analysis on the $\text{Si}[110]$ and $\text{Si}[111]$ interfaces with crystalline SiO_2 as well as on the interfaces with amorphous SiO_2 in Figure 4 and in supplementary material.⁵⁰

TABLE II. Charges of silicon atoms, calculated by ReaxFF_{SiO} in Si- SiO_2 system with the different oxidation number. Charges are estimates since exact values can vary, depending on deformations in the coordination sphere.

Oxidation number	Charge
0	0
+1	0.3
+2	0.8
+3	1.1
+4	1.6

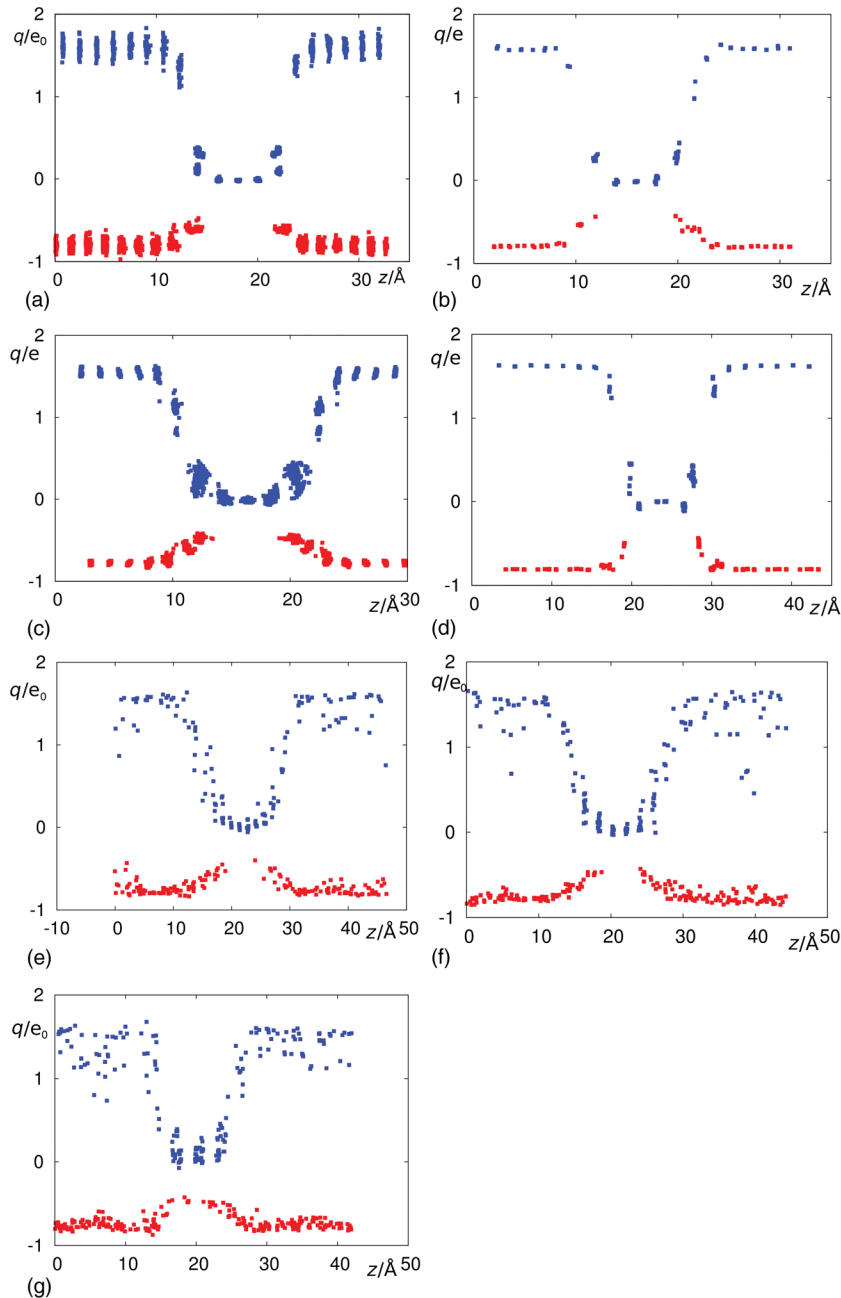


FIG. 4. The atomic charges in the modeled systems; atomic charges of silicon atoms are shown in blue color and oxygen charges in red color. (a) $\text{cSiO}_2[110]\text{A}$; (b) $\text{qSiO}_2[110]\text{A}$; (c) $\text{qSiO}_2[110]\text{B}$; (d) $\text{qSiO}_2[111]\text{A}$; (e) $\text{aSiO}_2[100]$; (f) $\text{aSiO}_2[110]$; (g) $\text{aSiO}_2[111]$.

All presented interfaces with crystalline SiO_2 are well defined with distinctive layers of silicon atoms with different oxidation numbers. The structure of $\text{qSiO}_2[110]\text{B}$ is disrupted more than other interfaces with $\text{Si}[110]$ and $\text{Si}[111]$ which is manifested in a larger spread of charges. In that case there is also a large deformation in silicon layer as can be seen from a large spread of atomic positions at the center of Figure 4(c). The deformation is also visible in Figure 2(d). The large spread of atomic positions caused merging of the layers occupied by atoms with oxidation number 0 and 1. Atomic charges at interfaces with aSiO_2 show continuous change from 0 in silicon layer to about $+1.6\text{ e}$ in aSiO_2 layer. In these cases, amorphous nature of interfaces is expected since interfaces are created with amorphous silicon-oxide phase. This is consistent with the charges we obtained in the case of interface $\text{cSiO}_2[100]$.²⁵ Figures 4(e)–4(g) indicate that there are silicon atoms in aSiO_2 layer with oxidation

number lower than $+4$. That is a consequence of stray Si-Si bonds in that layer.

IV. DEFECTS

A. Calculation of defects

Defects in the interfaces were identified, and molecular models of these defects were created by copying atomic coordinates of atoms around the defect. Hydrogen atoms are attached to all atoms at the edge of created molecular models in order to satisfy valencies of these atoms. Positions of these hydrogen atoms are optimized on MP2/6-31G(d) level while the rest of atoms were frozen. After that, the system was optimized again with all atoms frozen except few atoms, involved in the defect. The constraints, put by frozen atoms mimic the constraints, implied by a crystal lattice. The optimization on high-level *ab initio* calculation was used in order

to check bonding and structural motifs independently of ReaxFF_{SiO} parametrization. These calculations were done by using GAMESS program package.³¹

In all interfaces, after simulation of thermal treatment, the reconstruction of the interfaces generates defects in the form of three-coordinated [Si(3)] silicon atoms (dangling bond),^{20–22,34–37} five coordinated silicon atoms (floating bond),^{38–40} threefold-coordinated oxygen atom,^{41,42} or displaced oxygen atom.⁴²

B. Three-coordinated oxygen atom

The nature of three-coordinated oxygen atoms in the strained interface (Figure 4(b)) is further analyzed on model molecules, taken from the interface. Energy minimum in model molecules was searched among geometries created by putting oxygen atom between three-valence silicon atoms. The search for energy minimum is done by optimization with high-level *ab initio* MP2/6-31G(d) calculations. All possible geometries where the oxygen atom makes bridges between silicon atoms are tried as potential candidates for the potential energy surface minimum; however, all these geometries converged into the unique geometry (Figure 5).

In this geometry, the oxygen atom is positioned asymmetrically between the three silicon atoms, so the bond lengths between them are different. The identical bonding pattern is obtained from the optimization by the ReaxFF_{SiO}. The bonding pattern, obtained with the *ab initio* calculations, also confirms the finding obtained by optimization with the ReaxFF_{SiO} where the oxygen atom makes three bonds with three different bond orders.

C. Five-coordinated silicon atom

The another defect that was occurring in modeled interfaces was five-coordinated silicon atom. The optimization of small models with five coordinated Si atoms, taken from the ReaxFF_{SiO} optimized interfaces, resulted in migration of oxygen atom into the Si-Si bond and in change in bonding pattern. (Figure 6) The end-result is a regular four-coordinated silicon atom. Therefore, this type of defect is an artifact of the ReaxFF_{SiO}. Most of the five-coordinated silicon atoms are the result of interaction with oxygen atom over an elongated, partial bond. The sum of all bond orders on silicon atom in Si(5) defect is about 4 since most of the bonds

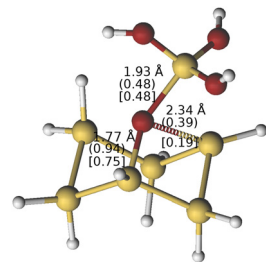


FIG. 5. The optimized model for interaction of oxygen atom with three dangling bonds. Bond lengths (in Ångströms) are shown next to the bonds, bond orders calculated with ReaxFF_{SiO} are shown in parenthesis, and bond orders, calculated according to Mayer definition, at MP2/6-31G(d) level are shown in square brackets.

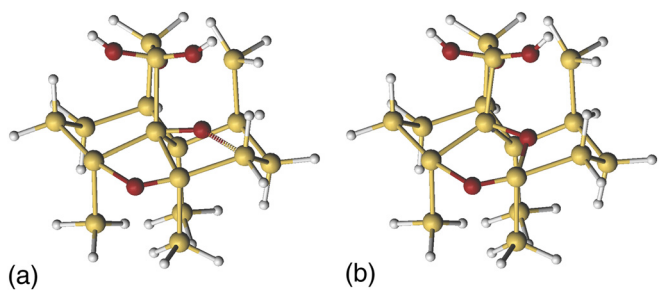


FIG. 6. The overcoordinated silicon atom at the interface of Si110 with cristobalite. (a) Geometry optimized by the ReaxFF; (b) the same geometry optimized by MP2/6-31G(d).

around that atom have partial character. Therefore, the large number of five-coordinated silicon atoms is the result of the parametrization of the ReaxFF_{SiO}.

D. Three-coordinated silicon atom

In the interfaces with β -cristobalite, there is a relatively low surface density of oxygen atoms, available for bonding with silicon atoms in the silicon slab. Therefore the interfaces of β -cristobalite with [110] and [111] surfaces of silicon contain Si(3) atoms (P_b centers). Modeled interfaces were created with pyramidal Si(3) atoms, as in silicon crystal, but with one bond missing. Thermal treatment and optimizations by the ReaxFF_{SiO} leaves that silicon atom in the pyramidal coordination, although thermal treatment deforms the coordination from the ideal pyramidal structure.

The Si(3) atom in silicon layer can trap electrons or holes^{21,23} resulting in positive (P_b^+) or negative (P_b^-) charge. Whether P_b center is positive or negative depends on the Fermi level. According to Lenahan and Conley,²³ the low Fermi level makes Si(3) unpopulated with electrons making it positive, P_b^+ ; in intermediate levels P_b center is populated with the single electron, and at the high Fermi level has two electrons and is negative, P_b^- . Unfortunately, the ReaxFF_{SiO} was parameterized for a neutral silicon only,²⁷ and it cannot describe P_b^+ and P_b^- . Therefore, the structure of Si(3) atom was also optimized inside a representative cluster (Si_7H_{15}) using *ab initio* calculations. The same clusters with the positive and negative charges were also optimized. The result is shown in Figure 7, upper row.

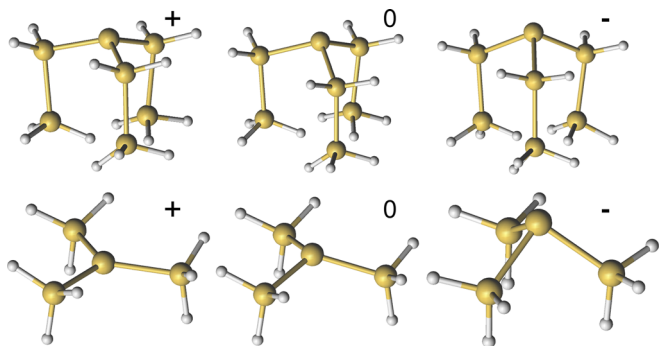


FIG. 7. A model for Si(3) defect. The upper row shows atoms around Si(3), taken from the interface model and optimized with constraints; the lower row shows optimized tris(trimethylsilyl)silane without constraints. Charges of the models are shown next to it.

Silicon atoms with the positive charge tend to migrate toward the planar configuration, and silicon atom with the negative charge makes more sharp angle pyramid. Since the silicon atoms around the pyramidal atom were constrained, the geometries of modeled Si(3) defects in Figure 7 could be the result of steric conditions coming from the bond-length of Si-Si bonds. Therefore, the geometries of *tris(trimethylsilyl)silane radical* (Si_4H_9) (Figure 7, the lower row) were also optimized without any constrictions in order to check the defect geometry in fully relaxed structures. The presented structures show the same trend as in the constrained structures (Figure 7, the upper row), although the differences between the structures with different charges are much more pronounced. In the structure with the positive charge the Si(3) atom lies almost in the plane with three neighboring silicon atoms. In order to check whether this out-of-plane deviation is an artifact, caused by the insufficient geometry convergence threshold, the geometry was reoptimized with the threshold decreased by an order of magnitude (10^{-5} Hr/Bohr for the largest component of gradient and 3.33×10^{-6} Hr/Bohr for RMS gradient). In separate calculation, the geometry of positively charged model for Si(3) atom is optimized from the initial geometry in which all silicon atoms lie in the plain. All mentioned calculations converged into a pyramidal geometry shown in Figure 7. Therefore we can conclude that in positive form, Si(3) atom forms almost planar trigonal coordination. There is no significant difference between geometries of pyramidal three-coordinated silicon atoms in the interface, obtained by the ReaxFF_{SiO} and the neutral three-coordinated silicon atom in the constrained model molecule, optimized with MP2/6-31G(d). Si-Si bonds tend to be shorter as charge increases toward positive values. The reason for this trend is a tendency of a three-coordinated silicon atom toward large-angle pyramidal structures. Since the base of pyramid is constrained, the large-angle pyramid is achieved by shortening Si-Si bonds.

The relative energies of the calculated models show that the negatively charged structures are the most stable (Table III). This makes the trend in energies: $\text{Si}(3)^- < \text{Si}(3)^0 < \text{Si}(3)^+$ which is opposite from the trend published by Lenahan *et al.*²³ Conclusions about the change of populations by Lenahan and Conley were drawn from EPR spectra and

TABLE III. The geometrical parameters of three-coordinated silicon atoms, obtained with the ReaxFF_{SiO} in the modeled interface and with MP2/6-31G(d) in model molecules (constrained Si_7H_{15} and in Si_4H_9). The geometrical parameters are h , the pyramid height; $r_{\text{Si-Si}}$, the silicon-silicon bond length; ΔE is the difference in energy with respect to the uncharged model.

Structure	$h/\text{\AA}$	$r_{\text{Si-Si}}/\text{\AA}$	$\Delta E/\text{eV}$
Interface, ReaxFF _{SiO}	1.04 ^a	2.30 ^a	
$\text{Si}_7\text{H}_{15}^+$	0.79 ^a	2.20 ^a	7.34 ^a
$\text{Si}_7\text{H}_{15}^0$	1.01 ^a	2.29 ^a	0 (reference)
$\text{Si}_7\text{H}_{15}^-$	1.21 ^a	2.38 ^a	-2.42 ^a
Si_4H_9^+	0.10	2.38	6.94
Si_4H_9^0	0.48	2.34	0 (reference)
Si_4H_9^-	1.27	2.36	-1.74

^aThe average value.

only a neutral form is EPR active, so there was no indication that $\text{Si}(3)^+$ should be more stable than $\text{Si}(3)^0$. Furthermore the same trend as ours is observed in calculations of Si(3) with interaction with oxygen atoms by Bloch.⁴³

There are two uncertainties about the stability of P_b in the Si-SiO₂ interface. The first uncertainty is in the charge on P_b defect. The energies, calculated with *ab initio* calculations, are obtained from small models while real P_b centers are located on the much larger systems where the charge can be delocalized and effectively alter the charge on three-coordinated silicon atom. Nonetheless, it was shown⁴⁴⁻⁴⁶ that the charge can accumulate on defects at Si-SiO₂ interface similarly as in localized models. The second uncertainty is in the electric field between silicon and silicon-oxide layers. The electronegativity of oxygen atoms in SiO₂ layer withdraws the charge making that layer more negative than the silicon layer. The electric field is also contributed by local charges on three-coordinated Si atom and point charges within the SiO₂ layer. The charges on the ideal Si-SiO₂ interface were estimated from the electron-equilibration method (within ReaxFFSiO₂ force field) and from *ab initio* calculations on clusters to about 0.01 Hr e⁻¹ Bohr⁻¹.^{47,48} See supplementary material for list of calculated charges.⁵⁰ In order to check the relative stability of three-coordinated silicon atoms in the electric field, we optimized models (Si_7H_{15} and Si_4H_9) in the electric field with different strengths. As can be seen in Figure 8, the differences in energy between charged and neutral Si_7H_{15} decreases as electric field increases. At the strongest field, used in calculations, differences in energy are still much larger than the differences in Fermi level where change in occupations of charged P_b defects was observed.²³ That indicates that the charge in the defect is delocalized, and only partially on Si(3), making it effectively less charged and/or the strength of the electric field felt by Si(3) is stronger than the estimated value. Unfortunately, strong electric fields cause instability in SCF convergence, so calculations with stronger electric fields were not done.

Nevertheless, these calculations demonstrate that the P_b^+ defect is less stable than the P_b defect which is less stable than the P_b^- defect, even in estimated electric field in Si-SiO₂ interfaces.

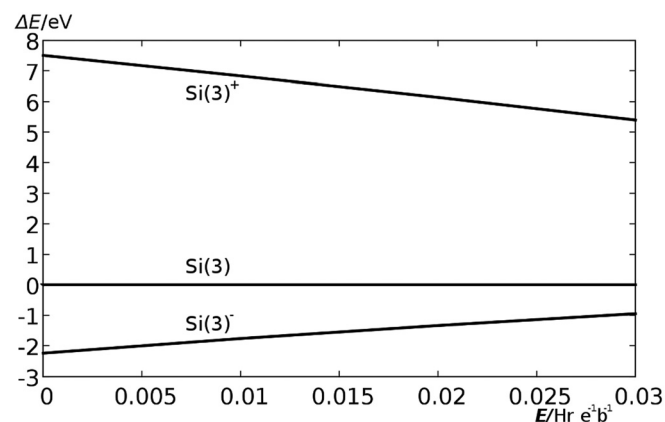


FIG. 8. The relative stability (ΔE) of positive $[\text{Si}(3)^+]$ and negative $[\text{Si}(3)^-]$ three-coordinated silicon with respect to the neutral form $[\text{Si}(3)^0]$ atom in modeled interfaces with respect to the electric field (E).

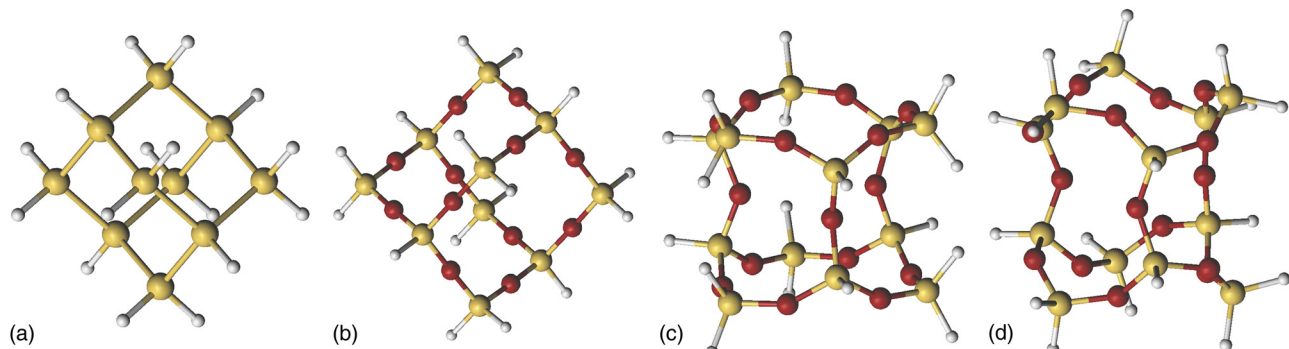


FIG. 9. Modeled systems used in calculation of the stress level caused by deformation. (a) Silicon; (b) β -cristobalite; (c) β -tridymite- D_{3d} constrained; (d) β -tridymite- C_3 constrained.

V. THE STRESS IN INTERFACES

A. Calculation of the stress

In order to quantify the stress in silicon and silicon oxide slabs, the stress was calculated by using the definition of Daruka *et al.*³² from the forces obtained with ReaxFF_{SiO}. In order to gain further insight in the nature of stress in interfaced systems, *ab initio* calculations were made with molecular clusters, cut from the silicon and silicon oxide crystal lattices. These clusters are shown in Figure 9. All border atoms were decorated with hydrogen in order to satisfy valencies on all atoms. Optimized structures were deformed (compressed/stretched) along z axis and gradients and energies were calculated on these deformed structures. Optimized structures were stretched and compressed up to 10% along z axis. Silicon and cristobalite models were constrained to the C_{2v} symmetry and the tridymite model was constrained to two different symmetries: C_3 and D_{3d} , respectively. These constraints do not allow large change in geometries that would make optimized geometries too different from the initial, crystal structure. Unfortunately, no small representation of the quartz structure could be made, that can be optimized into a structure still similar to the initial quartz structure.

B. The stress in modeled systems

The color-coded root-mean-square stress tensor is shown in Figure 10 for each atom in modeled systems. The Si[100]-cristobalite interface shows a very little stress. (Figure 10(a)) This result is in accordance with our previous results²⁵ where bond lengths in this interface were found to be closest to the bond lengths in the ideal crystals. The bonding pattern in this interface was also found to be the most disturbed among Si[100] interfaces. This interface is also more disturbed than any interface with crystalline silicon, considered in this paper. In most interfaces, the greatest strain is in the region of silicon oxide, next to the interface (Figs. 10(b), 10(c), 10(e), 10(f), 10(i), and 10(j)). Further from the interface, the level of strain drops. In interfaces with relatively large difference in lattice constants (Figures 10(i)–10(l)), the greatest strain is located on Si-O bonds in the silicon-oxide layer that is oriented parallel to the interface. The exception is the interface between Si[111] and

quartz where the silicon slab is buckled (Figure 10(f)). In that interface the strain is greatest in the areas where oxygen atoms are inserted in the silicon surface. In that case, the dominant strain pattern in the silicon oxide layer is vertical with respect to the direction of the silicon slab since the bonding pattern between silicon and silicon oxide bends silicon slab. In tridymite-Si[100] (Figures 10(k) and 10(l)) the greatest stress is on oxygen atoms, which are coordinated almost linearly, parallel to the interface. In that interface there is a significant mismatch (about 12%) in lattice constants of silicon and tridymite which makes tension in bonds that are parallel to the interface. The lowest stress is in the systems with amorphous SiO₂. These systems do not have constraints in lattice constants as in cases of crystalline SiO₂. Instead of a stress in preferred directions, a large stress in amorphous systems is localized on isolated atoms. On average, the stress is much lower in amorphous systems (under 8 Gpa) which is in accordance with calculations of Khalilov *et al.*⁴⁹

C. The susceptibility to stress

In each system considered, the silicon layer is less stressed than silicon oxide layers, despite the relatively large stress values in some cases of silicon oxide. The difference in stress values in silicon and silicon oxides is analyzed on the model systems of silicon and silicon-oxide (Figure 2). The calculation of energy gradients on these modeled systems revealed that stretching or compressing a silicon slab results in much lower forces than applying the same deformations on silicon oxide slabs. Figure 11 shows the energy gradient in the model clusters (Figure 2) (which is proportional to the stress), as a function of deformation. This explains a very low stress in silicon slabs sandwiched with silicon oxide layers. The large forces in deformed silicon-oxide are the consequence of the nature of Si-Si and Si-O bonds. Si-O bonds have much deeper and steeper potential well for dissociation than potential well of the Si-Si bond.²⁷

VI. CONCLUSION

Interfaces between silicon ([110] and [111]) and silicon-oxide were investigated for β -cristobalite (β c), and β -quartz (β q) as well as interfaces with amorphous silicon oxide forms. Defects and strain on these interfaces were investigated also.

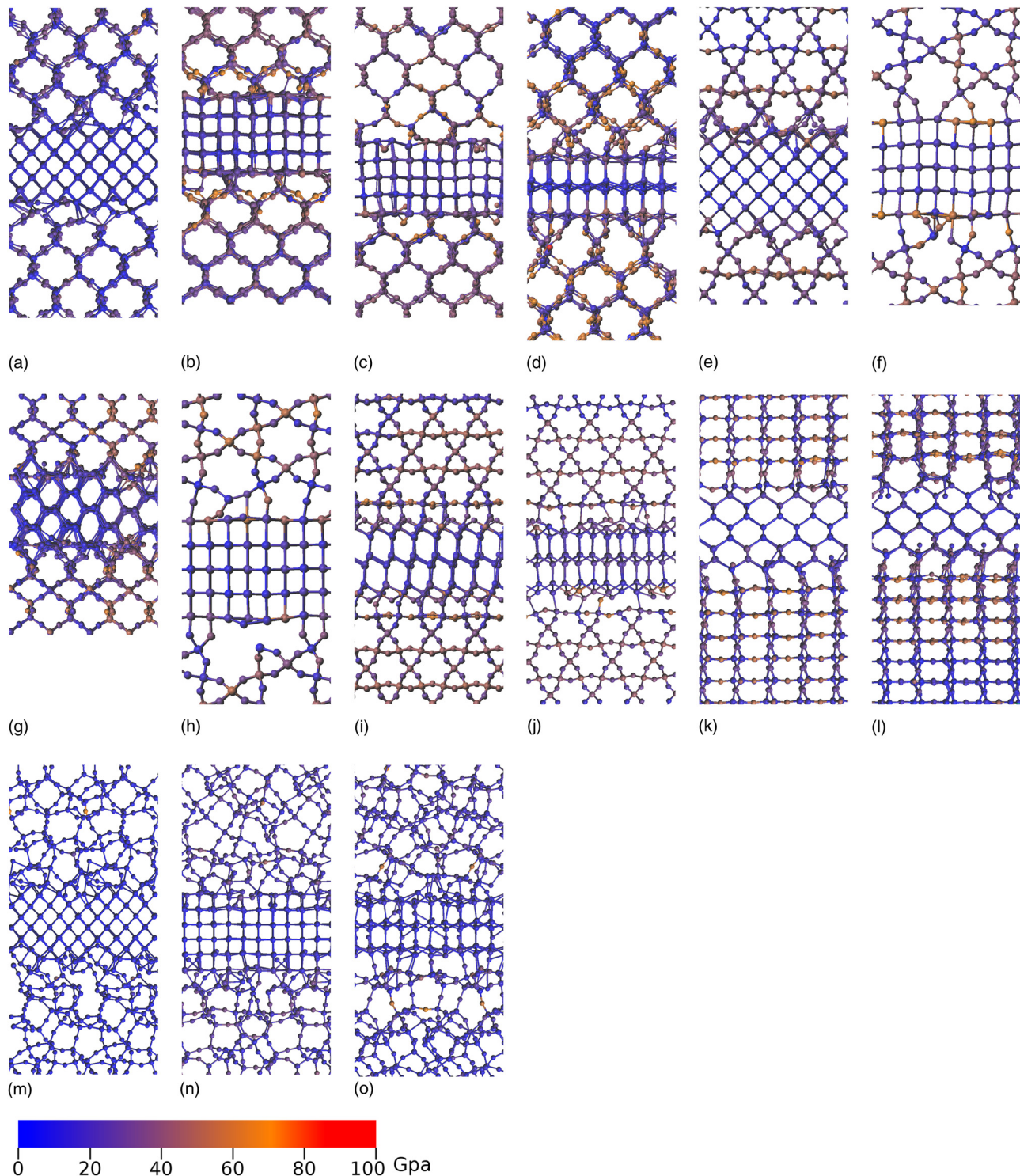


FIG. 10. The stress in the layers of interfaced slabs of silicon and silicon-oxide. (a) cSiO₂[100]; (b) cSiO₂[110]A; (c) cSiO₂[110]B; (d) cSiO₂[111]; (e) qSiO₂[100]; (f) qSiO₂[110]A; (g) qSiO₂[110]B; (h) qSiO₂[110]C; (i) qSiO₂[111]A; (j) qSiO₂[111]B; (k) tSiO₂[100]cb; (l) tSiO₂[100]r; (m) aSiO₂[100]; (n) aSiO₂[110]; (o) aSiO₂[111].

No interface with crystalline SiO₂ has been reorganized into the amorphous two-dimensional layer. Interfaces with large mismatches can create buckling of the silicon layer that shapes the layer into a wavelike pattern. Large mismatches can also create unusually bonded oxygen atoms, making one bond, that is the regular silicon-oxygen bond (about 1.8 Å) and two bonds that are strained (over 2.0 Å), partial bonds.

In all interfaces, the reconstruction of the interfaces generates defects in form of three-coordinated [Si(3)] silicon atoms (dangling bond, Pb defect), five coordinated silicon atoms (floating bond), threefold-coordinated oxygen atom, or displaced oxygen atom. Defects in the form of three-coordinated silicon atoms are most stable as negatively charged. Introduction of the electric field, caused by the

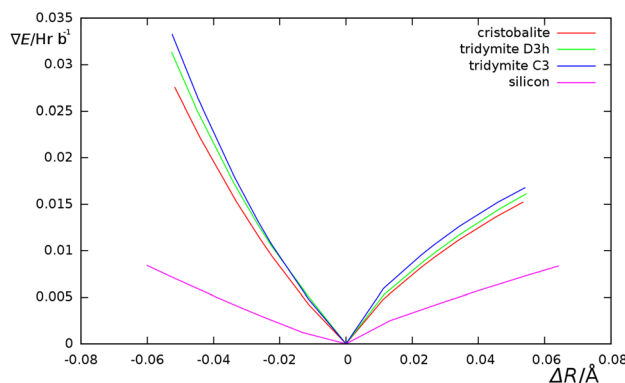


FIG. 11. The energy gradients on the deformed model systems that represent silicon and silicon oxide crystals. Deformations are represented as a mean bond length (R) stretching (positive values) or compressing (negative values).

interface, reduces the stability of negatively charged three-coordinated silicon atom.

The stress in the Si-SiO₂ systems is mostly contained in SiO₂ layer. In systems with a large mismatch in periodic constants, where bonding in SiO₂ layer is parallel to the interface, the stress is significantly contributed by these bonds. In the system where silicon layer is buckled, the greatest stress is near the oxygen atom that caused buckling. The analysis of susceptibility for stress showed that silicon has lower stress than silicon-oxide if put under the same strain.

ACKNOWLEDGMENTS

The authors wish to thank Adri van Duin for giving the ReaxFF_{SiO} parameters. This study has been partially funded by EU project NanoPV (FP7-NMP3-SL-2011-246331).

- ¹R. W. Cahn, *Electrochim. Soc. Interface* **14**, 15–16 (2005).
- ²A. V. Latyshev and A. L. Aseev, *Usp. Fizich. Nauk* **168**, 1126–1127 (1998).
- ³A. C. Diebold, D. Venables, Y. Chabal, D. Muller, M. Weldon, and E. Garfunkel, *Mater. Sci. Semicond. Proc.* **2**, 103–147 (1999).
- ⁴M. Ieong, B. Doris, J. Kedzierski, K. Rim, and M. Yang, *Science* **306**, 2057–2060 (2004).
- ⁵G. D. Wilk, R. M. Wallace, and J. M. Anthony, *J. Appl. Phys.* **89**, 5243–5275 (2001).
- ⁶Y. J. Chabal and L. C. Feldman, *Electrochim. Soc. Interface* **14**, 31–34 (2005).
- ⁷H. Akatsu, Y. Sumi, and I. Ohdomari, *Phys. Rev. B* **44**, 1616–1621 (1991).
- ⁸A. Ourmazd, D. W. Taylor, and J. A. Rentschler, *Phys. Rev. Lett.* **59**, 213–216 (1987).
- ⁹A. Munkholm, S. Brennan, F. Comin, and L. Ortega, *Phys. Rev. Lett.* **75**, 4254–4257 (1995).
- ¹⁰I. K. Robinson, K. Waskiewicz, and R. T. Tung, *Phys. Rev. Lett.* **57**, 2714–2717 (1986).

- ¹¹I. Takahashi, T. Shimura, and J. Harada, *J. Phys.: Condens. Matter* **5**, 6525–6536 (1993).
- ¹²F. J. Himpsel, F. R. McFeely, A. Taleb-Ibrahimi, and J. A. Yarmoff, *Phys. Rev. B* **38**, 6084–6096 (1988).
- ¹³M. M. B. Holl and F. R. McFeely, *Phys. Rev. Lett.* **71**, 2441–2444 (1993).
- ¹⁴A. Korkin, J. C. Greer, G. Bersuker, V. V. Karasiev, and R. J. Bartlett, *Phys. Rev. B* **73**, 165312 (2006).
- ¹⁵C. R. Helms and E. H. Poindexter, *Rep. Prog. Phys.* **57**, 791–852 (1994).
- ¹⁶H. Kageshima and K. Shiraishi, *Phys. Rev. Lett.* **81**, 5936–5939 (1998).
- ¹⁷P. J. Caplan, J. N. Helbert, B. E. Wagner, and E. H. Poindexter, *Surf. Sci.* **54**, 33–42 (1976).
- ¹⁸M. F. Chung and D. Haneman, *J. Appl. Phys.* **37**, 1879–1890 (1966).
- ¹⁹Y. Nishi, *Jpn. J. Appl. Phys.* **10**, 52–62 (1971).
- ²⁰M. Cook and C. T. White, *Phys. Rev. Lett.* **59**, 1741–1744 (1987).
- ²¹M. Cook and C. T. White, *Phys. Rev. B* **38**, 9674–9685 (1988).
- ²²A. Stirling, A. Pasquarello, J.-C. Charlier, and R. Car, *Phys. Rev. Lett.* **85**, 2773–2776 (2000).
- ²³P. M. Lenahan and J. F. Conley, Jr., *J. Vac. Sci. Technol. B* **16**, 2134–2153 (1998).
- ²⁴R. A. Street and N. F. Mott, *Phys. Rev. Lett.* **35**, 1293–1296 (1975).
- ²⁵G. Kovačević and B. Pivac, *Phys. Status Solidi A* **210**, 717–722 (2013).
- ²⁶A. C. T. van Duin, S. Dasgupta, F. Lorant, and W. A. Goddard III, *J. Phys. Chem. A* **105**, 9396–9409 (2001).
- ²⁷A. C. T. van Duin, A. Strachan, S. Stewman, Q. Zhang, X. Xu, and W. A. Goddard III, *J. Phys. Chem. A* **107**, 3803–3811 (2003).
- ²⁸J. C. Fogarty, H. M. Aktulga, A. Y. Grama, A. C. T. van Duin, and S. A. Pandit, *J. Chem. Phys.* **132**, 174704 (2010).
- ²⁹R. M. van Ginhoven, H. Jónsson, and R. L. Corrales, *Phys. Rev. B* **71**, 024208 (2005).
- ³⁰R. M. van Ginhoven and H. P. Hjalmarson, *Nucl. Instrum. Methods: Phys. Res. B* **255**, 183–187 (2007).
- ³¹M. W. Schmidt, K. K. Baldridge, J. A. Boatz, S. T. Elbert, M. S. Gordon, J. J. Jensen, S. Koseki, N. Matsunaga, K. A. Nguyen, S. Su *et al.*, *J. Comput. Chem.* **14**, 1347–1363 (1993).
- ³²I. Daruka, A.-L. Barabási, S. J. Zhou, T. C. Germann, P. S. Lomdahl, and A. R. Bishop, *Phys. Rev. B* **60**, R2150–R2153 (1999).
- ³³S. M. Shapiro, D. C. O’Shea, and H. Z. Cummins, *Phys. Rev. Lett.* **19**, 361–364 (1967).
- ³⁴A. Stesmans, *Appl. Phys. Lett.* **48**, 972–975 (1986).
- ³⁵W. Füssel, M. Schmidt, H. Angermann, G. Mende, and H. Flietner, *Nucl. Instrum. Methods: Phys. Res. A* **377**, 177–183 (1996).
- ³⁶L.-B. Luo, X.-B. Yang, F.-X. Liang, H. Xu, Y. Zhao, X. Xie, W.-F. Zhang, and S.-T. Lee, *J. Phys. Chem. C* **115**, 18453–18458 (2011).
- ³⁷L.-Å. Ragnarsson and P. Lundgren, *J. Appl. Phys.* **88**, 938–942 (2000).
- ³⁸L. Martin-Moreno and J. A. Verges, *Phys. Rev. B* **39**, 3445–3448 (1989).
- ³⁹C. F. Sanz-Navarro, S. D. Kenny, and R. Smith, *Nanotechnology* **15**, 692–697 (2004).
- ⁴⁰R. Biswas, B. C. Pan, and Y. Y. Ye, *Phys. Rev. Lett.* **88**, 205502-1–205502-4 (2002).
- ⁴¹A. Pasquarello, M. S. Hybertsen, and R. Car, *Nature* **396**, 58–60 (1998).
- ⁴²N. Richard, L. Martin-Samos, G. Roma, Y. Limoge, and J.-P. Crocombette, *J. Non-Cryst. Solids* **351**, 1825–1829 (2005).
- ⁴³P. E. Blochl, *Phys. Rev. B* **62**, 6158–6179 (2000).
- ⁴⁴K. Kutsuki, T. Ono, and K. Hirose, *Sci. Technol. Adv. Mater.* **8**, 204–207 (2007).
- ⁴⁵T. Ono, *Phys. Rev. B* **79**, 195326-1–195326-5 (2009).
- ⁴⁶C. H. Ben-Porat, O. Cherniavskaya, L. Brus, K.-S. Cho, and C. B. Murray, *J. Phys. Chem. A* **108**, 7814–7819 (2004).
- ⁴⁷G. Lucovsky, H. Yang, and H. Z. Massoud, *J. Vac. Soc. Technol. B* **16**, 2191–2198 (1998).
- ⁴⁸H. Z. Massoud, *J. Appl. Phys.* **63**, 2000–2005 (1988).
- ⁴⁹U. Khalilov, G. Pourtois, A. C. T. van Duin, and E. C. J. Neyts, *Phys. Chem. C* **116**, 21856–21863 (2012).
- ⁵⁰See supplementary material at <http://dx.doi.org/10.1063/1.4862809> for charges in qSiO₂[110]C, qSiO₂[110]C, and qSiO₂[111]B interfaces and for list of calculated charges, calculated on molecular clusters.